

# Spin-selective coherent light scattering from ion crystals

Maurizio Verde,<sup>1</sup> Ansgar Schaefer,<sup>1</sup> Benjamin Zenz,<sup>1</sup> Ziad Shehata,<sup>2</sup> Stefan Richter,<sup>2</sup> Christian T. Schmiegelow,<sup>3</sup> Joachim von Zanthier,<sup>2</sup> and Ferdinand Schmidt-Kaler<sup>1,4</sup>

<sup>1</sup>*QUANTUM, Institut für Physik, Universität Mainz, Staudingerweg 7, 55128 Mainz, Germany.*

<sup>2</sup>*AG Quantum Optics and Quantum Information,*

*Friedrich-Alexander-Universität Erlangen-Nürnberg, Staudtstraße 1, 91058 Erlangen, Germany.*

<sup>3</sup>*Departamento de Física, FCEyN, Universidad de Buenos Aires and IFIBA,*

*CONICET, Pabellón 1, Ciudad Universitaria, 1428 Ciudad de Buenos Aires, Argentina.*

<sup>4</sup>*Helmholtz-Institut Mainz, Staudingerweg 18, 55128 Mainz, Germany.*

We study collective light scattering from linear crystals with up to twelve  $^{40}\text{Ca}^+$  ions, acting as coherent single photon emitters. Light-scattering is induced by two-photon laser excitation, starting from the  $S_{1/2}$  to  $D_{5/2}$  quadrupole transition at 729 nm in combination with laser excitation of the  $D_{5/2}$  to  $P_{3/2}$  dipole transition at 854 nm, followed by a decay back to  $S_{1/2}$  via a single photon emission near 393 nm. The scattered intensity is recorded in the far field, featuring the interference of emitted light fields of the entire crystal. Furthermore, we demonstrate spin-dependent coherent scattering and unveil the time evolution of a previously encoded spin texture in a crystal employing the recorded dynamics of the spatial frequency components of the fringe pattern.

Emerging microscopic phenomena feature astonishing collective properties, and trapped ion crystals offer unique opportunities for their classical or quantum simulation. This includes the study of defect formation in (structural) phase transitions [1–4] but also magnetic phase transitions, which have been implemented first using a quantum simulator with two ions [5], but now employ scaled-up systems for uncovering a plethora of magnetic phases [1, 6–12]. There is high interest in quantum simulations with even larger and eventually two-dimensional systems [13–15], as these would allow for analyzing frustrated spin models that feature elusive properties but are notoriously hard to predict from numerical simulations [16]. In a typical quantum simulation run, spins are initialized, their mutual interactions are switched on, and after a desired evolution time, the spin projection is recorded for each site by imaging laser-induced fluorescence on a spatial-resolving detector [17]. The interesting question is whether spin textures, as the outcome of a quantum simulation run, can be recorded alternatively. Could spin-correlations be directly and in-situ detected from observing interferences in the intensity of collectively scattered photons?

Here, we demonstrate coherent scattering of light from an array of ions, each of them acting as a single photon emitter (SPE). We are measuring the intensity  $I(z)$  in the far field, described by the photon correlation function  $g^{(1)}(z, z)$ . Our method is able to reveal spin-textures, using the benefits of Fourier optics, which is known for resolving spatial frequencies. We determine the latter from the patterns, and in this way find the distances between the SPEs with equal spin state. Note, that our method realizes an in-situ detection [18, 19], which we implement in a background-free fashion. The contrast of the interference pattern uncovers the degree of coherence and the indistinguishability of the photons emitted in the array of SPEs, which might be difficult to identify

otherwise [20–23].

In this letter, first we describe the experimental setup of the ion trap, the laser interactions to excite  $^{40}\text{Ca}^+$  ion crystals and the detection of photons. We then outline the scheme for obtaining spin-dependent scattering and describe the data analysis to reveal both, the SPE-array configuration and its spin order. Finally, we are initializing the crystal with specific spin orders, and record the real-time evolution of the multi-spin interference pattern.

We use a linear Paul trap to confine linear crystals of  $^{40}\text{Ca}^+$  under ultra-high vacuum conditions. The trap is built in X-blade geometry [24] with a diagonal electrode distance of 960  $\mu\text{m}$  and with eleven DC segments of width 200  $\mu\text{m}$ . We apply the radio frequency of  $\Omega_{RF}/(2\pi) = 30.04 \text{ MHz}$  to achieve secular frequencies along the two radial directions of  $\omega_{R1,R2}/(2\pi) = \{2.26, 2.59\} \text{ MHz}$ . We adapt the DC voltages to  $\{+5 \text{ V}, 0, 0, 0, 0, u, 0, 0, 0, 0, +5 \text{ V}\}$  for the segments with  $u = -8 \text{ V}$  in case of three ions to get an axial trap frequency of  $\omega_z/(2\pi) = 0.72 \text{ MHz}$ , and relax this potential to  $\omega_z/(2\pi) = 0.58 \text{ MHz}$  using  $u = -1.5 \text{ V}$  for trapping crystals with up to twelve ions.

The directions of the two exciting laser beams are in the x-z plane and impinge the crystal under  $+45^\circ$  for the beam at 729 nm and under  $-45^\circ$  for the beam at 854 nm, while emitted photons near 393 nm are collected in opposite x-direction by the objective, see Fig. 1(i). The scattered light is focused by the objective at a distance of about 127 cm on a slit of width 1.4 mm (not shown in Fig. 1), whereas the LINCAM detector (Photonscore Inc.) is positioned further downstream in the far field at 170 cm distance.

During loading, we use the  $S_{1/2}$  to  $P_{1/2}$  transition near 397 nm for Doppler cooling, while a repumper near 866 nm empties the metastable  $D_{3/2}$  level, see Fig. 1(ii). A flip-mirror is placed in the setup to image the ion crystal on an EMCCD camera (both not shown in Fig. 1(i))

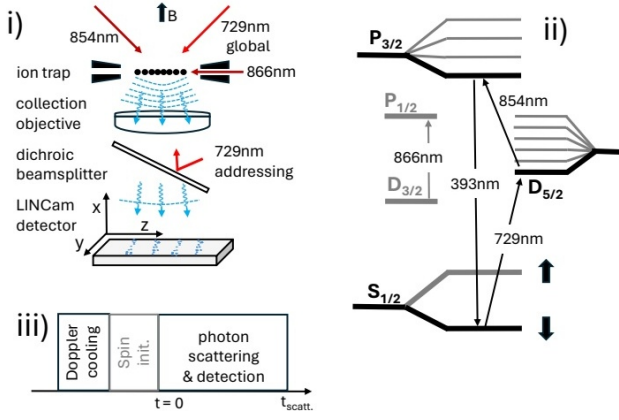


FIG. 1. i) Sketch of the experimental setup: A linear crystal of  $^{40}\text{Ca}^+$  ions is exposed to laser fields (729 nm/854 nm/866 nm) with beam waist sizes of (25  $\mu\text{m}$ /80  $\mu\text{m}$ /80  $\mu\text{m}$ ), respectively. Scattered photons near 393 nm are collected by the NA = 0.3 objective (Sill, S6ASS2241) onto a multi-channel plate detector LINCam at a distance of 170 cm. For single ion addressing, a beam near 729 nm is reflected off the dichroic beam splitter, and focused by the objective to a waist size of 2  $\mu\text{m}$ . ii) Levels and transitions in  $^{40}\text{Ca}^+$ :  $S_{1/2}$  Zeeman levels  $m = \pm 1/2$  serve as spin up / spin down state, respectively. Spin-dependent scattering is achieved by two-photon excitation with wavelengths near 729 nm and 854 nm. iii) Pulse sequence for spin-dependent detection: After Doppler cooling (397 nm/866 nm), the spin is initialized by the addressing beam (729 nm), and then the spin-dependent scattering is recorded under illumination by the global beams (729 nm/854 nm) while repumping the residual population via the short-lived  $P_{1/2}$  level (866 nm) to  $S_{1/2}$ .

for probing the number of ions during loading as well as prior and posterior to any of the measurements. A magnetic field of 0.996 mT is applied in  $x$ -direction to provide a quantization axis, and to separate the Zeeman levels of the  $S_{1/2}$  state by 27.92 MHz.

To realize the light scattering experiments, the beam near 397 nm is switched off, and the 729 nm laser excites the narrow-band  $S_{1/2}$ ,  $m = -1/2$  ( $\equiv \downarrow$ ) to  $D_{5/2}$ ,  $m = -5/2$  transition, while simultaneously driving the transition near 854 nm, which quenches the long-lived  $D_{5/2}$  via the  $P_{3/2}$  state back to  $S_{1/2}$ , by the emission of a single photon at 393 nm, as shown in Fig. 1(ii). If the detuning, the Rabi frequencies and the polarization are properly chosen, we implement an almost closed-cycle back into the  $S_{1/2}$ ,  $m = -1/2$  state. In this spin selective scattering regime, the strengths of both laser fields are  $\Omega_{729}/(2\pi) = 0.302 \pm 0.006$  MHz and  $\Omega_{854}/(2\pi) = 2.48 \pm 0.15$  MHz, respectively. They have been determined independently, from recording Rabi oscillations in the first case and from observing the depletion dynamics of the  $D_{5/2}$  level in the latter. Under these conditions, we experimentally find a rate for photons at 393 nm of about 400 Hz per ion, free of background, with 20 Hz dark counts from the LINCam.

By increasing the Rabi frequency of the beam near 854 nm by a factor of two the light scattering rate is raised. But the probability of pumping into, and exciting from the  $S_{1/2}$ ,  $m = +1/2$  ( $\equiv \uparrow$ ) state becomes larger, thus the detection scheme gradually loses its spin-selectivity. The resulting continuous light scattering regime is employed for sub-Doppler cooling [25] when tuning the frequency of the 729 nm laser below the quadrupole transition by  $\Delta/(2\pi) \sim 1.55$  MHz. We determine the ion temperature from resolved sideband spectroscopy and find it to be about 70  $\mu\text{K}$ . This is well below the measured Doppler limit of 0.5 mK. Modelling the three-level system [25, 26] we find an effective two-level system with linewidth  $\Gamma_{\text{theo}}/(2\pi) = 1.10 \pm 0.28$  MHz what would lead to a cooling limit [27] of  $80 \pm 5$   $\mu\text{K}$ , where the uncertainty comes from the estimated Rabi frequencies.

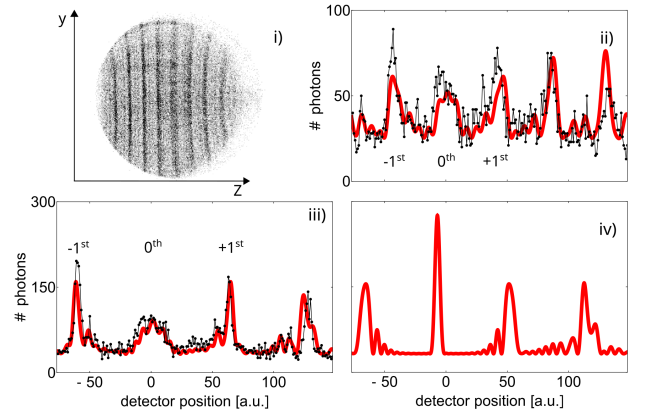


FIG. 2. (i) LINCam image with interference pattern from a  $N = 6$  ion linear crystal, diameter 17 mm. Summing up over the  $y$ -axis leads to interference fringes, here displayed for the case of linear crystals with (ii)  $N = 6$  and (iii)  $N = 12$  ions. The data acquisition time is 240 s. The model function (red) takes into account the independently determined ion positions, the laser beam profiles and a quadratic phase shift due to optical aberration, see text for details. (iv) Model function evaluated for the twelve ion crystal, but excluding the quadratic phase shift.

As the ions constitute a linear array of emitters almost perfectly localized and at rest, the interference patterns are expected to form lines on the spherical outgoing waves. The projection of the sphere onto the detector surface plane leads to interference patterns oriented along the  $y$ -axis, see Fig. 2(i). Summing up data in the central part over the  $y$ -direction, we obtain interference fringes as shown in Fig. 2(ii) and (iii), (see online material for data sets for crystals with  $N = 4$  to 12).

The separation between the  $0^{\text{th}}$  diffraction order and the  $\pm 1^{\text{st}}$  diffraction order is determined by the inverse of the inter-ion separation  $l_0$  which is at the center of a linear 12-ion crystal 3.26  $\mu\text{m}$  for an axial trap frequency of 0.58 MHz. However, the inter-ion distance in a harmonic

potential increases for ions further out of the center. Consequently, the  $\pm 1^{\text{st}}$  diffraction order is split up in several peaks, nicely visible e.g. in the case of a 12-ion crystal in Fig. 2(iii). Here, the  $\pm 1^{\text{st}}$  orders at positions  $\pm 65$  display a series of side peaks towards the center.

Remarkably, also the  $0^{\text{th}}$  diffraction order consist of many peaks, instead of one single narrow line. In an ideal optical far field setup, the  $0^{\text{th}}$  diffraction order of a linear array of emitters placed on the  $z$ -axis would not feature any path length differences. We conjecture an optical aberration by the light collection objective, causing a parasitic phase shift for rays emitted by SPEs displaced off the optical axis by a distance  $z$ . This aberration effect shows up especially when light is collected over a larger field as it is the case for crystals with large ion number. According to Zernike's description of lens imperfections, we model a quadratic parasitic phase shift  $\phi(z-z_0) = az^2$  for the SPE phases, where  $z_0$  accounts for an alignment offset.

To model the fringe pattern for an array of  $N$  point-like emitters we sum up their fields:

$$I = c_1 \left| \sum_{i=1}^N E_i \right|^2 + c_2. \quad (1)$$

The term with prefactor  $c_1$  denotes the normalized coherent part of the electric field and the second term with  $c_2$  the incoherently scattered part. The coherently emitted field by an ion at  $\mathbf{r}_i$  at detector position  $\mathbf{d}$  reads

$$E_i(\mathbf{d}, \mathbf{r}_i) = e^{ia(z_i-z_0)^2 - (\mathbf{r}_i/w_0)^2} \times e^{-i(\frac{2\pi}{\lambda}|\mathbf{d}-\mathbf{r}_i|)}. \quad (2)$$

The first term describes the aberration-induced quadratic phase shift discussed above, and an intensity-mask which is stemming from the finite waist of the 729 nm illumination, while the waist of the beam at 854 nm is much larger. The wave front curvature of the illumination beams leads to a negligible phase shift. The second term describes the path-length induced phase shifts for the light emitted at  $\lambda = 393$  nm. Optimum fit to the data is found for  $z_0 = 9 \mu\text{m}$  and  $a = 0.015 \text{ rad}/\mu\text{m}^2$ . This corresponds to a shift of  $\pi$  for an SPE off-center by  $\pm 15 \mu\text{m}$ . Taking this quadratic phase into account, and adapting with three values for the overall amplitude, contrast and magnification of interference fringes for the entire data set, we achieve good agreement with the data, see Fig 2(ii,iii). This model function is plotted in Fig 2(iv), now excluding the parasitic quadratic phases. Here, the  $0^{\text{th}}$  diffraction order collapses into a narrow peak, whereas the  $\pm 1^{\text{st}}$  orders display the inhomogeneous distribution of distances between ions, with a series of peaks in the direction towards the  $0^{\text{th}}$  diffraction order. For  $N = 12$ , the distances  $l$  between ions vary from the outermost right to the left-hand one like  $\{4.71, 3.94, 3.58, 3.39, 3.29, 3.26, 3.29, 3.39, 3.58, 3.94, 4.71\} \mu\text{m}$  [28].

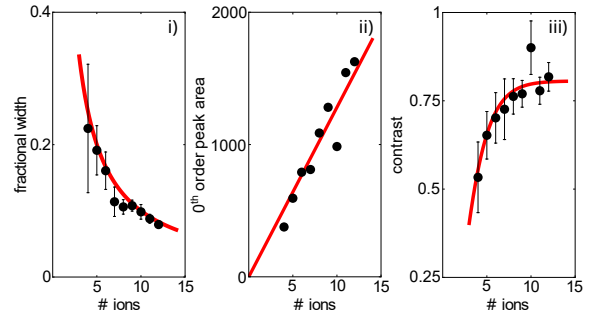


FIG. 3. (i) Fractional width, measured for crystals with  $4 \leq N \leq 12$  ions trapped in a 0.58 MHz axial potential. The expected  $1/N$  dependence is plotted (red), no free parameters. (ii) Photon counts integrated over the  $0^{\text{th}}$  order peak showing a linear increase with  $N$  (red). (iii) Contrast of the interference fringes versus the number of ions  $N$ . The dependence on  $N$  is described by a model function  $k_{\text{exp}}C(N)$ , see text for details.

We start by analyzing the fractional width of the  $0^{\text{th}}$  diffraction order and find agreement with the expected scaling with  $1/N$ , see Fig. 3(i). Here, the fractional width is defined by the width of the  $0^{\text{th}}$  diffraction order divided by the distance to the  $\pm 1^{\text{st}}$  diffraction order. Moreover, the total photon count in the  $0^{\text{th}}$  order peak increases linearly with the number of ions  $N$  in the crystal. Furthermore, we observe that the contrast of the interference fringes  $c_1/(c_1 + c_2)$  increases with  $N$  and then saturates for crystals with  $N > 8$ .

We model the far field intensity  $I$  [29, eq. 13.48], leaving aside the aberration from the light collection lens and the intensity mask considered in Equ. 2 but investigating mechanisms for loss of interference contrast:

$$\sum_{i,j=1}^N e^{-i\mathbf{q}(\mathbf{r}_i-\mathbf{r}_j)} \langle e^{i\mathbf{q}\mathbf{u}_j} e^{-i\mathbf{q}\mathbf{u}_i} \rangle \times C \times \langle S_{P,S}^{i\dagger} S_{P,S}^j \rangle. \quad (3)$$

The three terms correspond to three different effects all affecting the contrast of the fringe pattern: The first term describes the Debye-Waller (DW) factor, the second covers the fraction of spin combinations  $C$  which are leading to interference, and the last one denotes the relative fraction of coherently, above incoherently scattered light.

The first term contains ion equilibrium positions  $\mathbf{r}_i$ , their thermal and quantum fluctuations  $\mathbf{u}_i$  about these positions and the momentum transfer  $\mathbf{q}$ . We have chosen a geometry which leads to a partly compensated photon recoil in the absorption and subsequent emission event, see Fig. 1(i), and correspondingly only a small coupling to the motional degrees of freedom, characterized by single ion Lamb-Dicke parameters  $\eta_{(R1,R2,z)} = \{0.025, 0.023, 0.013\}$ . Also, as the ion crystal is cooled to sub-Doppler temperatures, the fluctuations are reduced almost the

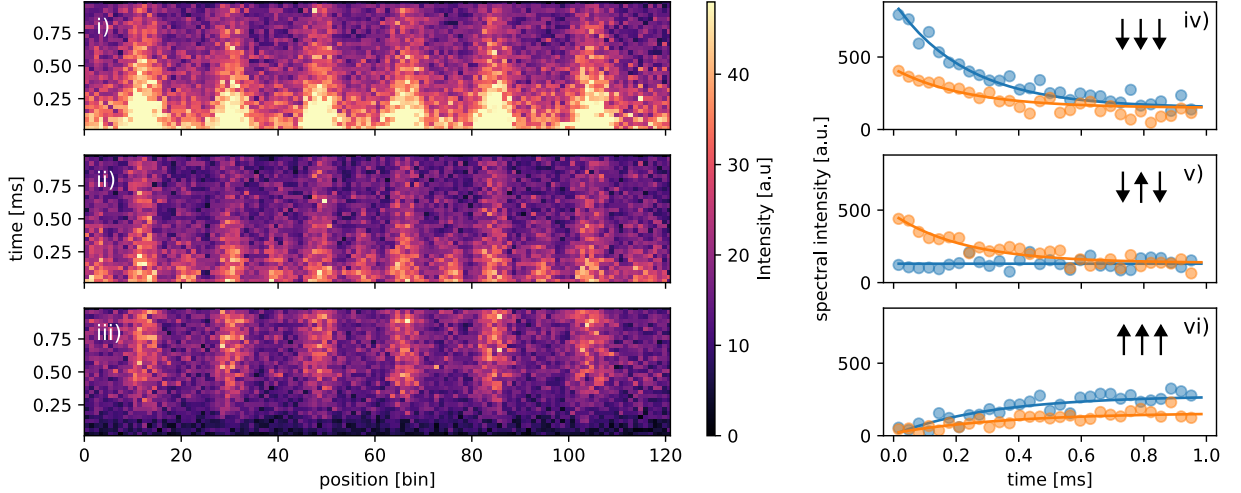


FIG. 4. Interference patterns observed from spin-initialized three-ion crystals with data acquisition time 1 ms, repeated for 150,000 times. Three plots on the left side show the number of detected photons in each bin position (x-axis) vs. the scattering time  $t_{scatt}$  (y-axis) for spin configuration initialization in (i):  $\{\downarrow, \downarrow, \downarrow\}$ , (ii):  $\{\downarrow, \uparrow, \downarrow\}$ , and (iii):  $\{\uparrow, \uparrow, \uparrow\}$ , respectively. The three plots on the right side display over time the intensity of the different spatial frequencies of the three-ion crystals, corresponding to the different inter-ion distances with ion in state  $\downarrow$ . Error bars are within the size of the dots. For the initial configuration  $\{\downarrow, \downarrow, \downarrow\}$  in (iv), we observe two spatial frequencies which decay as a function of time. In the case of  $\{\downarrow, \uparrow, \downarrow\}$  in (v), one Fourier frequency is present at the beginning and then decays, while the other one is barely visible throughout the observation time. Initializing the ion crystal to  $\{\uparrow, \uparrow, \uparrow\}$  in (vi), no spatial frequencies are observed initially, nonetheless they appear over time due a small leakage in the fluorescence cycle.

quantum limit. The loss of visibility due to the DW factor [30] is evaluated from the recoil-induced displacements of the ions from equilibrium position in terms of eigenvectors of the ion crystal's motion [28]. With increasing ion number two effects take place: the summation over a higher number of  $3N-3$  modes and the increased mass of  $N$  ions which contribute to common modes of vibration. Finally, our calculation of the DW yields a value close to unity, when taking into account an ion crystal at  $\omega/(2\pi)=0.58$  MHz and a temperature of about 70  $\mu$ K, as measured for a single ion under the same laser illumination conditions.

The second term contains the fraction of ion pairs in the spin  $\downarrow$  state  $C$ . As we do not initialize the spin states in the measurements shown in Fig. 2, each ion in the crystal may either be in the  $\downarrow$  state or in the  $\uparrow$  state, where the latter does almost not scatter light. Therefore, out of the  $2^N$  different possible combinations for an  $N$ -ion crystal in total, only the  $N$  combinations, where one ion is in  $\downarrow$  state, and the situation with all ions in the  $\uparrow$  state, do not contribute to the interference pattern. This leads to a factor of  $C(N) = 1 - \frac{N}{2^N} - \frac{1}{2^{(N+1)}}$ .

The last term describes the amount of coherently scattered photons, as only they contribute to the interference pattern.  $S_{p,s}^i$  and  $S_{p,s}^{i\dagger}$  denote the lowering and raising operators of ion  $i$  from the  $S_{1/2}$  state to the  $P_{3/2}$  state, respectively. We have conducted a 3-level simulation involving also the  $D_{5/2}$  state and found a contrast reduction

by about  $0.930 \pm 0.001$ , taking the experimental parameters into account. The combination of all three terms describes the contrast. We fit the model to the data in Fig. 3(iii), using the combinatorial factor  $C(N)$  together with a prefactor  $k_{exp}$  that takes into account the reduction due to incoherently scattered light. The finding  $k_{exp} = 0.80 \pm 0.02$  is close to the theoretical prediction.

Finally, we extend our study to the situation where we initialize the spin state of the ions in the linear crystal individually and observe the fringe patterns obtained from different spin textures. Deterministic preparation is done by addressing single ion spins with an additional beam near 729 nm focused to a 2  $\mu$ m waist, see Fig. 1(i). In this way, we are able to initialize all the different  $2^N = 8$  spin-patterns.

A time-resolved measurement on a spin-initialized crystal consists of repeating a sequence of three steps: Doppler-cooling, spin-initialization, and finally, observation of photon scattering for 1 ms by exciting at 729 nm and 854 nm, as described above. As before, we sum photon detection events over the y-direction on the LINCcam detector. Now, time stamps of the detected photons are also recorded as the LINCcam receives a trigger when the photon scattering time starts. Such data allow for examining the time-evolution of the diffraction pattern, which displays how spin textures develop, see Fig. 4(i,ii,iii). This dynamics occurs due to a small leakage in the fluorescence cycle, pumping all spin textures eventually into

equilibrium.

If we initialize the spins to the setting  $\{\downarrow, \downarrow, \downarrow\}$  all ions emit light, and we observe two spatial Fourier frequencies in the far field fringe pattern, corresponding to the distance between the outermost ions ( $2 \times l_0$ ) and that for neighboring ions ( $l_0 = 5.17 \mu\text{m}$ , at  $\omega/(2\pi) = 0.72 \text{ MHz}$ ). They show up strongest directly after the initialization and decay for longer times, see Fig. 4(iv). As expected, the Fourier amplitude corresponding to a distance of  $l_0$  is higher by a factor of  $2.0 \pm 0.2$ , as compared with that for the distance  $2 \times l_0$ . On the other hand, if the crystal is initialized in  $\{\downarrow, \uparrow, \downarrow\}$ , only one Fourier frequency appears, corresponding to the distance  $2 \times l_0$ . For an initialization with  $\{\uparrow, \uparrow, \uparrow\}$ , no light is initially scattered. Yet, scattered light is observed with time due to the leakages in the fluorescence cycle. We prove that the experimental data (see online material) show the expected Fourier components also for all other five spin configurations, thus witnessing the initialized spin-texture.

When spin states are flipped due to optical pumping processes, we observe this in-situ from the amplitude decay or increase of a specific Fourier component, see Fig. 4(iv,v,vi). The rates for the dynamics  $\tau_{\downarrow\uparrow} = 0.24 \pm 0.01 \text{ ms}$ , and in reverse  $\tau_{\uparrow\downarrow} = 0.33 \pm 0.01 \text{ ms}$ , respectively, are extracted from the entire data set. The recorded time variation of the respective Fourier amplitudes clearly shows the ability to observe in-situ the evolution of spin-textures in ion crystals.

In the future, we plan to employ collective spin-dependent scattering as an investigation tool for observing quantum phase transitions in analogue quantum simulations. Furthermore, we will improve the count rate using a pair of high numerical aperture light collection objectives. Another challenge comes from the inhomogeneous distribution of the ion distances in a harmonic trap. Two solutions are intended: Either using a laser waist size smaller than the total extension of the ion crystal, such that only the equidistantly distributed center part contributes to the interference fringes. Alternatively, we may tailor the axial potential in the micro-segmented trap [21, 31, 32] such that equidistant ion crystals are formed.

We acknowledge financial support by the Deutsche Forschungsgemeinschaft (DFG, German Research Foundation) – Project-ID 429529648 – TRR 306 QuCoLiMa (“Quantum Cooperativity of Light and Matter”), by the Dynamics and Topology Centre funded by the State of Rhineland-Palatinate, the Erlangen Graduate School in Advanced Optical Technologies (SAOT) and thank Daniel Wessel and Dr. Jonas Vogel for careful reading. A. S., B. Z. and M. V. contributed equally to this work.

- [1] R Islam, EE Edwards, K Kim, S Korenblit, C Noh, H Carmichael, G-D Lin, L-M Duan, C-C Joseph Wang, JK Freericks, et al. Onset of a quantum phase transition with a trapped ion quantum simulator. *Nat. Comm.*, 2 (1):377, 2011.
- [2] B.-W. Li, Y.-K. Wu, Q.-X. Mei, R. Yao, W.-Q. Lian, M.-L. Cai, Y. Wang, B.-X. Qi, L. Yao, L. He, Z.-C. Zhou, and L.-M. Duan. Probing critical behavior of long-range transverse-field ising model through quantum kibble-zurek mechanism. *Phys. Rev. X Quantum*, 4: 010302, 2023.
- [3] S Ulm, J Roßnagel, G Jacob, C Degünther, ST Dawkins, UG Poschinger, R Nigmatullin, A Retzker, MB Plenio, F Schmidt-Kaler, et al. Observation of the kibble-zurek scaling law for defect formation in ion crystals. *Nat. Comm.*, 4(1):2290, 2013.
- [4] K Pyka, J Keller, HL Partner, R Nigmatullin, T Burgermeister, DM Meier, K Kuhlmann, A Retzker, Martin B Plenio, WH Zurek, et al. Topological defect formation and spontaneous symmetry breaking in ion coulomb crystals. *Nat. Comm.*, 4(1):2291, 2013.
- [5] Axel Friedenauer, Hector Schmitz, Jan Tibor Glueckert, Diego Porras, and Tobias Schätz. Simulating a quantum magnet with trapped ions. *Nat. Phys.*, 4(10):757–761, 2008.
- [6] R. Blatt and C. F. Roos. Quantum simulations with trapped ions. *Nat. Phys.*, 8(4):277–284, April 2012. ISSN 1745-2481. doi:10.1038/nphys2252.
- [7] Jiehang Zhang, Paul W Hess, A Kyprianidis, Petra Becker, A Lee, J Smith, Gaetano Pagano, I-D Potirniche, Andrew C Potter, Ashvin Vishwanath, et al. Observation of a discrete time crystal. *Nat.*, 543(7644):217–220, 2017.
- [8] Jiehang Zhang, Guido Pagano, Paul W Hess, Antonis Kyprianidis, Patrick Becker, Harvey Kaplan, Alexey V Gorshkov, Z-X Gong, and Christopher Monroe. Observation of a many-body dynamical phase transition with a 53-qubit quantum simulator. *Nat.*, 551(7682):601–604, 2017.
- [9] Crystal Noel, Pradeep Niroula, Daiwei Zhu, Andrew Risinger, Laird Egan, Debopriyo Biswas, Marko Cetina, Alexey V Gorshkov, Michael J Gullans, David A Huse, et al. Measurement-induced quantum phases realized in a trapped-ion quantum computer. *Nat. Phys.*, 18(7):760–764, 2022.
- [10] P Jurcevic, H Shen, P Hauke, C Maier, T Brydges, C Hempel, BP Lanyon, Markus Heyl, R Blatt, and CF Roos. Direct observation of dynamical quantum phase transitions in an interacting many-body system. *Phys. Rev. Lett.*, 119(8):080501, 2017.
- [11] K Kim, S Korenblit, R Islam, E E Edwards, M-S Chang, C Noh, H Carmichael, G-D Lin, L-M Duan, C C Joseph Wang, J K Freericks, and C Monroe. Quantum simulation of the transverse ising model with trapped ions. *New Jour. Phys.*, 13:105003, October 2011. doi:10.1088/1367-2630/13/10/105003.
- [12] Ch Schneider, Diego Porras, and Tobias Schaetz. Experimental quantum simulations of many-body physics with trapped ions. *Rep. Progr. Phys.*, 75(2):024401, 2012. doi: 10.1088/0034-4885/75/2/024401.
- [13] Florian Kranzl, Manoj K. Joshi, Christine Maier, Tiff

- Brydges, Johannes Franke, Rainer Blatt, and Christian F. Roos. Controlling long ion strings for quantum simulation and precision measurements. *Phys. Rev. A*, 105:052426, 2022.
- [14] S.-A. Guo, Y.-K. Wu, J. Ye, L. Zhang, W.-Q. Lian, R. Yao, Y. Wang, R.-Y. Yan, Y.-J. Yi, Y.-L. Xu, B.-W. Li, Y.-H. Hou, Y.-Z. Xu, W.-X. Guo, C. Zhang, B.-X. Qi, Z.-C. Zhou, L. He, and L.-M. Duan. A site-resolved 2d quantum simulator with hundreds of trapped ions under tunable couplings. *arXiv:2311.17163*, 2023.
- [15] J. Welzel, F. Stopp, and F. Schmidt-Kaler. Spin and motion dynamics with zigzag ion crystals in transverse magnetic gradients. *Jour. Phys. B: Atomic, Molecular and Optical Physics*, 52(2), 2018.
- [16] Alejandro Bermudez, Juan Almeida, Ferdinand Schmidt-Kaler, Alex Retzker, and Martin B Plenio. Frustrated quantum spin models with cold coulomb crystals. *Phys. Rev. Lett.*, 107:207209, 2011.
- [17] Colin D. Bruzewicz, John Chiaverini, Robert McConnell, and Jeremy M. Sage. Trapped-ion quantum computing: Progress and challenges. *Appl. Phys. Rev.*, 6(2):021314, 2019.
- [18] Chen-Lung Hung, Xibo Zhang, Li-Chung Ha, Shih-Kuang Tung, Nathan Gemelke, and Cheng Chin. Extracting density-density correlations from in situ images of atomic quantum gases. *New Jour. Phys.*, 13(7):075019, 2011.
- [19] Andika Putra, Daniel L Campbell, Ryan M Price, Subhadeep De, and IB Spielman. Optimally focused cold atom systems obtained using density-density correlations. *Rev. Sci. Instr.*, 85(1), 2014.
- [20] U Eichmann, James C Bergquist, JJ Bollinger, JM Gilligan, Wayne M Itano, David J Wineland, and MG Raizen. Young’s interference experiment with light scattered from two atoms. *Phys. Rev. Lett.*, 70(16):2359, 1993.
- [21] Sebastian Wolf, Julian Wechs, Joachim von Zanthier, and Ferdinand Schmidt-Kaler. Visibility of young’s interference fringes: Scattered light from small ion crystals. *Phys. Rev. Lett.*, 116(18):183002, 2016.
- [22] G Cerchiari, G Araneda, L Podhora, L Slodička, Y Colombe, and R Blatt. Motion analysis of a trapped ion chain by single photon self-interference. *Appl. Phys. Lett.*, 119(2), 2021.
- [23] Petr Obšil, Adam Lešundák, Tuan Pham, Gabriel Araneda, Martin Čížek, Ondřej Číp, Radim Filip, and Lukáš Slodička. Multipath interference from large trapped ion chains. *New Jour. Phys.*, 21(9):093039, 2019.
- [24] S. Wolf. PhD thesis, Johannes Gutenberg-Universität Mainz, 2019.
- [25] I Marzoli, J I Cirac, R Blatt, and P Zoller. Laser cooling of trapped three-level ions: Designing two-level systems for sideband cooling. *Phys. Rev. A*, 49(4):2771, 1994.
- [26] Dirk Reiss, Albrecht Lindner, and Rainer Blatt. Cooling of trapped multilevel ions: A numerical analysis. *Phys. Rev. A*, 54(6):5133–5140, December 1996. ISSN 1094-1622. doi:10.1103/physreva.54.5133.
- [27] H Janacek. PhD thesis, University of Oxford, 2015.
- [28] D.F.V. James. Quantum dynamics of cold trapped ions with application to quantum computation. *Appl. Phys. B: Lasers and Optics*, 66(2):181–190, February 1998. ISSN 1432-0649. doi:10.1007/s003400050373.
- [29] G. S. Agarwal. Quantum optics. Cambridge University Press, Cambridge, UK, 2013. ISBN 978-1-107-00640-9.
- [30] W. M. Itano, J. C. Bergquist, J. J. Bollinger, D. J. Wineland, U. Eichmann, and M. G. Raizen. Complementarity and young’s interference fringes from two atoms. *Phys. Rev. A*, 57(6):4176–4187, June 1998. ISSN 1094-1622. doi:10.1103/physreva.57.4176.
- [31] V. Kaushal, B. Lekitsch, A. Stahl, J. Hilder, D. Pijn, C. Schmiegelow, A. Bermudez, M. Müller, F. Schmidt-Kaler, and U. Poschinger. Shuttling-based trapped-ion quantum information processing. *AVS Quantum Sci.*, 2: 014101, March 04 2020.
- [32] T. Ruster, C. Warschburger, H. Kaufmann, C. T. Schmiegelow, A. Walther, M. Hettrich, A. Pfister, V. Kaushal, F. Schmidt-Kaler, and U. G. Poschinger. Experimental realization of fast ion separation in segmented paul traps. *Phys. Rev. A*, 90:033410, September 10 2014. doi:10.1103/PhysRevA.90.033410.